SPH approach for simulating hydro-mechanically processes with large deformations and variable permeabilities

M. Gholami Korzani[a], S. A. Galindo-Torres[a,b], A. Scheuermann[a], D. J. Williams[a]

[a]*School of Civil Engineering, The University of Queensland, St Lucia (Brisbane) QLD 4072, Australia*
[b]*School of Engineering,University of Liverpool, Liverpool L69 3BX, United Kingdom*

Abstract

A simulation framework based on Smooth Particle Hydrodynamics is introduced to model problems involving the interaction between flowing water and soil deformation. Changes in soil porosity and associated permeability are automatically adjusted within this framework. The framework's capabilities are presented and discussed for three geotechnical problems caused by flowing water. The comparison between simulation results and experiments shows that SPH with the proposed concept is capable of quantitatively simulating the hydro-mechanical processes beyond limit state with satisfactory agreement. To improve the computational stability, a correction procedure and a new algorithm for the selection of the optimal time step are introduced.

Keywords: variable porosity and permeability; Smoothed Particle Hydrodynamics (SPH); soil-water interaction; elastic-plastic constitutive model; Geomechanics.

1. Introduction

Many deformation problems in geotechnical engineering involve the influence of flowing water on the soil structure initiating local soil movements, which are frequently the beginning of a chain of processes leading to a complete failure of the geotechnical structure. The large deformations occurring in the failing zone significantly alter the porosity of the soil with consequential changes in density and permeability, affecting in return the overall hydro-mechanical behaviour of the soil and thus the further evolution of the process. One main reason for these changes in porosity is the tendency of soil to dilate during shear deformation. The introduction of this porosity effect into numerical frameworks is challenging and frequently not possible as large deformations need to be simulated to fully capture the consequences from these porosity changes.

Based on Biot's theory of poroelasticity, porosity variations are the direct result from the deformations of the solid skeleton, which is a complex reaction to both, changes in water pressure and effective stress [47]. Terzaghi's one-dimensional consolidation theory is a special case of the Biot's theory. As a general result, stress and strain states have impacts on the coupled fluid-solid behaviours. When high permeable soils, such as sands and gravels, are studied, pore water pressure variations due to large deformation are instantaneous and temporary, and as a consequence negligible. However, volumetric deformations leading to changes in porosity can be significant and permanent.

Many studies focus on the liquefaction of soils due to excess pore water pressure as a result of seismic excitation. Di and Sato [10] used a FE-FD coupled method to simulate the liquefaction due to dynamic cyclic loading and introduced a variable void ratio based on a consolidation theory for cyclic loadings. A similar approach, using the concept of Biot's theory, was used by [33, 36, 40] to define the porosity and permeability as a function of the deformation to investigate the behaviour of primarily low permeable saturated soils undergoing large deformation. Wang and Xu [48] studied experimentally the effect of strain on the permeability of sandstone.

Email address: m.gholamikorzani@uq.edu.au (M. Gholami Korzani)

Although, there are numerous studies available related to the hydro-mechanical behaviour of granular media and the associated effects on porosity and consequently permeability, numerical tools which allow the numerical simulation of large deformations also considering the positive feedback from changes in permeability is still scarce [34]. The aim of this study is, therefore, the introduction of an appropriate numerical approach for simulating large deformations of granular soils under the influence of flowing water considering also the changes in permeability the associated effects on the process. To achieve this goal, a variable porosity and permeability concept on continuum scale is introduced and implemented in an open-source code called PersianSPH[1], which is a numerical tool based on Smoothed Particle Hydrodynamics (SPH) for geotechnical investigations [14, 15]. Three distinct experimental case studies are used to verify the numerical tool and to demonstrate the potential of this new numerical tool.

2. Numerical approach

The advent of high-performance computational resources has made the use of particle-based methods, which are comparably slower than meshed ones and less affordable for scientific computing. Amongst several mesh-free methods, SPH were spreadly implemented and applied in the scientific community. SPH is a Lagrangian mesh-free particle method that was developed in the late 70s [24], and was originally applied for the purpose of numerical analysis in astrophysics [21]. Nowadays, this method is being used in a broad range of research fields including solid mechanics [17, 19], hydrodynamics [13, 51] and also geotechnical engineering [5, 16, 35, 52]. This method is beneficial for solving several typical problems such as moving boundaries (e.g. free-surface flow), complex boundary geometries and large deformations. In essence, SPH scheme uses an interpolation technique, which is based on the integral representation of a field function $f(\boldsymbol{x})$, to describe the continuum. To employ this concept of integral representation numerically, the computational domain should be then discretized into a finite number of integration points (also called particles), and a smoothing function (so-called kernel), $W(\boldsymbol{x}-\boldsymbol{x}', h)$, is also deployed. Subsequently, the initial fundamental equation in SPH can be shown in the form of summation over particles within the support domain of the kernel as follows:

$$f(\boldsymbol{x_a}) = \sum_{b=1}^{N} m_b \frac{f_b}{\rho_b} W(r_{ab}, h) \tag{1}$$

where the subscript a denotes the focal integration point (particle), and the subscript b is for particles in the neighborhood of the particle a; N is total number of neighbour particles. h, m and ρ, represent the smoothing length, mass, and density, respectively. Details of the gradient approximation and other mathematical formulations in the SPH framework are comprehensively provided in [21, 23].

Kernels must satisfy several conditions to be allowed taking the place of Dirac Delta in the original integral form of SPH. The three most important conditions are: (1) *normalization condition*: the integration of the kernel over the volume is equal to one; (2) *Delta function property*: the kernel is similar to the Dirac Delta function when the smoothing length approaches zero; and (3) *compactness*: the effective area (non-zero) of the kernel is compact (limited). The choice of the kernel has impacts on the accuracy, efficiency, and stability of the SPH scheme [8, 15, 42]. Throughout the present study, the most widely-used kernel which is the cubic spline, is considered [30].

2.1. Water model

Water can be simulated in SPH as a slightly compressible viscous fluid through the Weakly Compressible SPH (WCSPH) approach [28, 30]. The SPH discretization of the conservation of mass and momentum in fluids (so-called the Navier-Stokes equations) are given by [32]:

the continuity equation:

$$\frac{d\rho_a}{dt} = \rho_a \sum_{b=1}^{N} \frac{m_b}{\rho_b} v_{ab}^{\alpha} \frac{\partial W_{ab}}{\partial x_a^{\alpha}}, \quad \text{where} \quad v_{ab}^{\alpha} = v_a^{\alpha} - v_b^{\alpha} \tag{2}$$

[1] http://korzani.wixsite.com/persiansph

the momentum equation:

$$\frac{dv_a^\alpha}{dt} = -\sum_{b=1}^{N} m_b \left(\frac{p_a + p_b}{\rho_a \rho_b}\right) \frac{\partial W_{ab}}{\partial x_a^\alpha} + \sum_{b=1}^{N} \frac{m_b(\mu_a + \mu_b) v_{ab}^\alpha}{\rho_a \rho_b} \left(\frac{1}{r_{ab}} \frac{\partial W_{ab}}{\partial r_{ab}}\right) + g_a^\alpha \tag{3}$$

where g and v are body force and velocity of each particle, respectively. Each particle also carries a mass, m, and density, ρ. N is total number of neighbour particles of the fluid phase. An equation of state (EOS) must be used in WCSPH to explicitly calculate thermodynamic pressure. The EOS used in this paper is proposed by Batchelor for water [12, 30]:

$$p = \frac{\rho_0 c_s^2}{7} \left(\left(\frac{\rho}{\rho_0}\right)^7 - 1\right) \tag{4}$$

where c_s is the speed of sound, and ρ_0 denotes the density at rest (initial condition). For further details of fluids simulation, refer to [15]

2.2. Soil model

The mass conservation equation (Eq. (2)) is also valid for soils in the continuum mechanics; however, the general form of the momentum equation should be used in the following form: particles:

$$\frac{dv_i^\alpha}{dt} = \sum_{j=1}^{M} m_j \left(\frac{\sigma_i^{\alpha\beta} + \sigma_j^{\alpha\beta}}{\rho_i \rho_j}\right) \frac{\partial W_{ij}}{\partial x_i^\beta} + g_i^\alpha \tag{5}$$

where $\sigma^{\alpha\beta}$ is the stress tensor which requires a proper soil constitutive model. M is total number of neighbour particles in the soil phase. In this paper, an elastic-perfectly plastic model in the conjunction of the Drucker-Prager failure criterion is employed as the soil constitutive relationships [7]. This type of soil modelling was proposed in SPH in [5, 6], and details of the derivation can be found in [6, 7]. However, the essential equations are provided in this paper.

By use of the generalized Hooke's law and Jaumann rate, an elastic material stress tensor can be written by:

$$\dot{\sigma}^{\alpha\beta} - \sigma^{\alpha\gamma}\dot{\omega}^{\beta\gamma} - \sigma^{\gamma\beta}\dot{\omega}^{\alpha\gamma} = 2G\dot{e}^{\alpha\beta} + K\dot{\epsilon}^{\gamma\gamma}\delta^{\alpha\beta} \tag{6}$$

where K, G, $\dot{\epsilon}^{\gamma\gamma}$ and $\dot{e}^{\alpha\beta}$ denote the bulk modulus, shear modulus, volumetric and deviatoric strain-rates, respectively. $\delta^{\alpha\beta}$ is Kronecker's delta, $\delta^{\alpha\beta} = 1$ if $\alpha = \beta$ and $\delta^{\alpha\beta} = 0$ if $\alpha \neq \beta$. $\dot{\epsilon}^{\alpha\beta}$ and $\dot{\omega}^{\alpha\beta}$ are the total strain-rate and rotation-rate tensors defined in SPH as:

$$\dot{\epsilon}^{\alpha\beta} = \frac{1}{2}\left(\frac{\partial v^\alpha}{\partial x^\beta} + \frac{\partial v^\beta}{\partial x^\alpha}\right) \Rightarrow \dot{\epsilon}_i^{\alpha\beta} = \frac{1}{2}\sum_{j=1}^{M}\left(\frac{m_j}{\rho_j}(v_j^\alpha - v_i^\alpha)\frac{\partial W_{ij}}{\partial x_i^\beta} + \frac{m_j}{\rho_j}(v_j^\beta - v_i^\beta)\frac{\partial W_{ij}}{\partial x_i^\alpha}\right) \tag{7}$$

$$\dot{\omega}^{\alpha\beta} = \frac{1}{2}\left(\frac{\partial v^\alpha}{\partial x^\beta} - \frac{\partial v^\beta}{\partial x^\alpha}\right) \Rightarrow \dot{\omega}_i^{\alpha\beta} = \frac{1}{2}\sum_{j=1}^{M}\left(\frac{m_j}{\rho_j}(v_j^\alpha - v_i^\alpha)\frac{\partial W_{ij}}{\partial x_i^\beta} - \frac{m_j}{\rho_j}(v_j^\beta - v_i^\beta)\frac{\partial W_{ij}}{\partial x_i^\alpha}\right) \tag{8}$$

where the subscripts i and j are used to describe SPH soil particles as opposed to water ones. Subsequently, the non-associated flow rule is employed in this study to simulate the plastic behaviour of soils in large deformation utilizing the Drucker-Prager's criterion in plane-strain condition:

$$Y(I_1, J_2) = \sqrt{J_2} + \alpha I_1 = k \tag{9}$$

$$\alpha = \frac{\tan\phi}{\sqrt{9 + 12\tan^2\phi}} \quad \text{and} \quad k = \frac{3c}{\sqrt{9 + 12\tan^2\phi}} \tag{10}$$

where I_1 is the first invariant of the stress tensor, and J_2 denotes the second invariant of the deviatoric stress tensor. c and ϕ represent the cohesion and internal friction angle of soil, respectively. In addition, a plastic potential function is required for the non-associated flow rule which is defined by:

$$g = \sqrt{J_2} + 3I_1 \sin\psi \tag{11}$$

where ψ is the dilatancy angle, and A zero dilatancy angle of the non-associated flow rule indicates that the material is plastically incompressible [6]. After combining Eqs. (6), (9) and (11), the elastic-plastic soil stress tensor for particle i in the SPH framework can be written as [6, 7],

$$\frac{d\sigma_i^{\alpha\beta}}{dt} = \sigma_i^{\alpha\gamma}\dot{\omega}_i^{\beta\gamma} + \sigma_i^{\gamma\beta}\dot{\omega}_i^{\alpha\gamma} + 2G\dot{e}_i^{\alpha\beta} + K\dot{\epsilon}_i^{\gamma\gamma}\delta^{\alpha\beta} - \dot{\lambda}_i\left[9K\sin\psi\,\delta^{\alpha\beta} + \frac{G}{\sqrt{J_2}}s_i^{\alpha\beta}\right], \tag{12a}$$

$$\dot{\lambda}_i = \frac{3\alpha K\dot{\epsilon}_i^{\gamma\gamma} + (G/\sqrt{J_2})s_i^{\alpha\beta}\dot{\epsilon}_i^{\alpha\beta}}{27\alpha K\sin\psi + G} \tag{12b}$$

where $\dot{\lambda}$ is the rate of the so-called plastic multiplier, λ, which is dependent on the state of stress and load history. $s^{\alpha\beta}$ denotes the deviatoric stress. By using Eq. (12a), a proper stress tensor in the momentum equation (Eq. (5)) is introduced for modelling soil behaviour in SPH. For further details of soil constitutive equations, refer to [14].

2.3. Soil-water interaction

When water is seeping through a soil sample, it applies the seepage force on soil particles in the form of a frictional drag force. Simultaneously, it reduces the effective stress due to the accumulated pore water pressure. To simulate soil-water interaction in this study, the proposed method in [14] is employed, which couples the dynamics of fluid and soil by means of a buoyancy force plus a seepage force. To consider the effective stress in this approach, the submerged (buoyant) unit weight is used in the case of the fully submerged sample (water level is above the soil sample surface). Otherwise, the total unit weight should be used. The seepage force can be described either by Darcy's law (in the case of laminar flow condition) or the Forchheimer equation (in the case of turbulent flow condition). Nonetheless, the seepage force in either descriptions mentioned above, can be defined by a single equation as (a force per unit of volume of soil):

$$\boldsymbol{f}^{seepage} = a(\boldsymbol{v}_{water} - \boldsymbol{v}_{soil})\gamma_w + b|\boldsymbol{v}_{water} - \boldsymbol{v}_{soil}|(\boldsymbol{v}_{water} - \boldsymbol{v}_{soil})\gamma_w \tag{13}$$

where $\boldsymbol{v}$ is the velocity vector of either soil or water particles and γ_w denotes the unit weight of the water. In the case of Darcy's law, a and b are $1/k$ and zero, respectively, where k denotes the hydraulic conductivity of the soil. The Kozeny-Carman equation can be used to calculate the hydraulic conductivity based on the particle size distribution as follows:

$$k = \frac{1}{180}\frac{n^3}{(1-n)^2}\frac{g}{\nu}d_e^2 \tag{14}$$

where n and d_e stand for the porosity and effective particle diameter of soil, respectively. g and ν are the gravity acceleration and water kinematic viscosity. When the turbulent flow is governing, the approach of Den Adel [9, 41] was used to calculate these coefficients as:

$$a = \alpha\frac{(1-n)^2}{n^3}\frac{\nu}{gd_{15}^2} \quad \text{and} \quad b = \beta\frac{1}{n^2}\frac{1}{gd_{15}} \tag{15}$$

where d_{15} denotes the particle size at 15% in the particle size distribution. As discussed and validated in [14], $\alpha = 150$ and $\beta = 0.4$ were used in this paper.

The artificial viscosity Π, as extensively explained in [14], is used in this study to prevent unphysical penetration of particles approaching each other. Moreover, the artificial stress, $R_{ij}^{\alpha\beta}f_{ij}^n$, is employed to eliminate the tensile instability by introducing a short-range artificial force between soil particles [14]. Consequently,

the final momentum equations for each phase by considering the soil-water interaction can be summarized as:

the momentum equation for the soil phase:

$$\frac{dv_i^\alpha}{dt} = \sum_{j=1}^{M} m_j \left(\frac{\sigma_i'^{\alpha\beta} + \sigma_j'^{\alpha\beta}}{\rho_i^s \rho_j^s} + R_{ij}^{\alpha\beta} f_{ij}^n + \Pi_{ij}\delta^{\alpha\beta} \right) \frac{\partial W_{ij}}{\partial x_i^\beta} + g_i^\alpha + \sum_{a=1}^{N} m_a \frac{f_{ia}^{seepage\ \alpha}}{\rho_i^s \rho_a} W_{ia} \tag{16}$$

the momentum equation for the water phase:

$$\frac{dv_a^\alpha}{dt} = -\sum_{b=1}^{N} m_b \left(\frac{p_a + p_b}{\rho_a \rho_b} + \Pi_{ab} \right) \frac{\partial W_{ab}}{\partial x_a^\alpha} + \sum_{b=1}^{N} \frac{m_b(\mu_a + \mu_b) v_{ab}^\alpha}{\rho_a \rho_b} \left(\frac{1}{r_{ab}} \frac{\partial W_{ab}}{\partial r_{ab}} \right) + g_a^\alpha - \sum_{i=1}^{M} m_i \frac{f_{ia}^{seepage\ \alpha}}{\rho_i^s \rho_a} W_{ia} \tag{17}$$

where the subscripts i and j represent soil particles while a and b are used for water particles. N and M are the total number of particles in the neighbourhood of a focal particle in water and soil phases, respectively. ρ^s stands for the submerged soil density as defined in Gholami Korzani et al. [14] for managing the effective stress.

2.4. Variable permeability concept

Failure of geotechnical structures usually occurs with large deformation. Generally, deformation is defined as the transformation of a body from one configuration to another one. This transformation in porous media, such as in soils, can lead to either increase or decrease of the body volume. Since the volume of soil particles in a soil sample is constant by the assumption of rigid soil particles and mass conservation, only the void volume varies when the body volume (the total soil sample volume) changes. Under consideration of a Representative Elementary Volume, the volumetric strain is defined by:

$$\epsilon_v = \frac{V - V_o}{V_o} \tag{18}$$

where V_o and V are the initial and current volume of the body, respectively. The porosity in soils is given by:

$$n = \frac{V_V}{V} = 1 - \frac{V_S}{V} \tag{19}$$

where V_V and V_S are the volume of voids and solids, respectively. By assuming that solids volume is fixed ($V_S = const$), the porosity can be derived as:

$$n = \frac{n_o + \epsilon_v}{1 + \epsilon_v} \tag{20}$$

where n_o denotes the initial porosity. It is worth noting that the volumetric strain is the trace of the strain tensor, $\epsilon^{\gamma\gamma}$, in the tensorial notation.

By this approach, the porosity is a function of the deformation which is quite significant in the process associated with the failure and post-failure of geotechnical structures. As a and b in Eq. (13) are functions of the porosity, the hydraulic conductivity or permeability can accordingly vary during the deformation.

2.5. Time integration

A modified explicit Verlet scheme [14] is utilized in this paper to integrate Eqs. (2), (12a), (16) and (17). The selection of the time step value is strongly dependent on three limitations as explained in [14]. The last condition is on the force per unit mass:

$$\Delta t \leq 0.25 \min(\sqrt{h_i/a_i}) \tag{21}$$

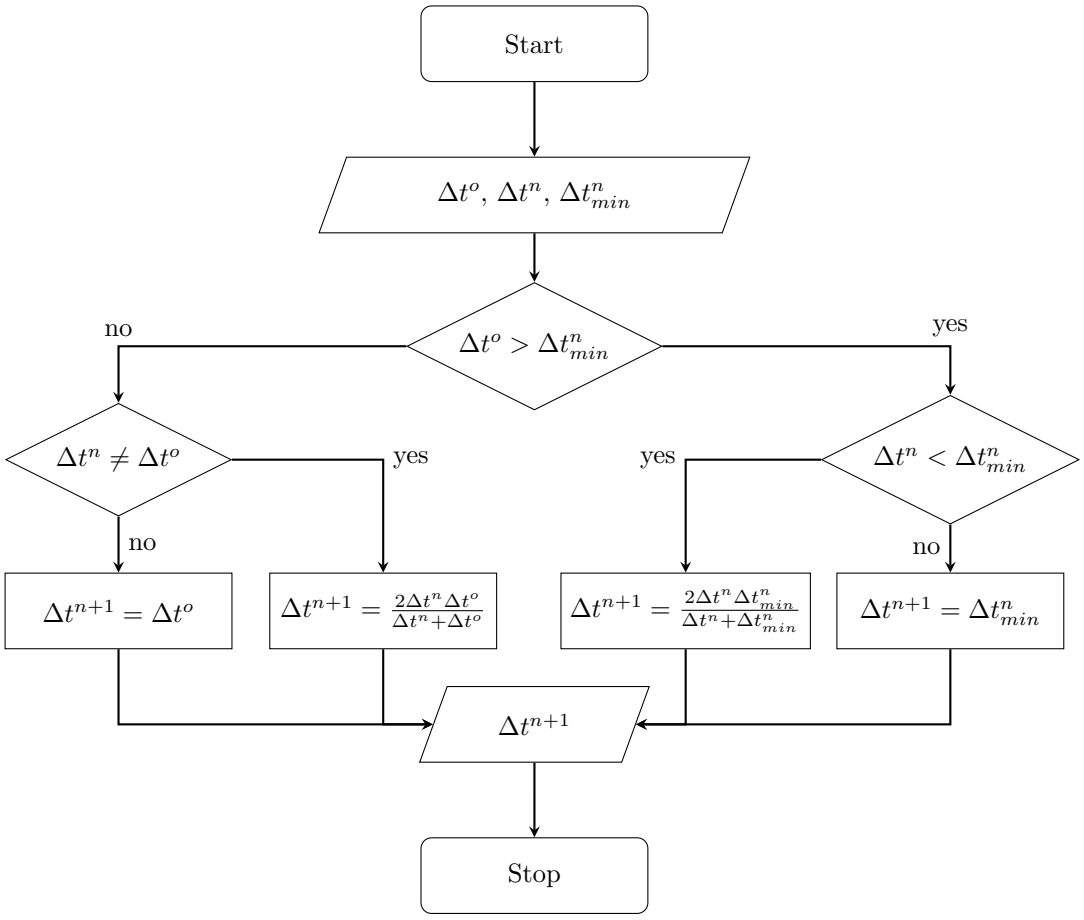

Figure 1: Algorithm for modifying time step value during a simulation

where a_i is the acceleration of the particle i. This limitation needs to be checked at each time step for every particle. However, this guideline on the time step value was suggested originally for a single phase SPH [29]. The body force caused by the seepage force on both, soil and water particles, can be significant in the magnitude during the failure or high-velocity water infiltration. Therefore, a larger body force as the result of the interaction requires a smaller time step value. Furthermore, a low hydraulic conductivity can reduce the time step value considerably. As a result, the factor of 0.25 in Eq. (21) is no longer a suitable value to keep simulations stable and accurate. After several simulations in this study, 0.005 was found to be an appropriate compromise between performance and stability in order to be able to model soil-water interaction. Nonetheless, remarkable changes in the time step value Δt during a simulation can also generate numerical instabilities and errors. Hence, the following algorithm is proposed in this study, to smoothly modify time step value all over the duration of a simulation:
where Δt^o, Δt^n and Δt^{n+1} denote the time step value at the initial time $t = 0$, current time t, and advance time $(t + \Delta t^{n+1})$, respectively. Δt^n_{min} is the minimum time step value calculated using Eq. (21) for all particles at the current time.

Based on this algorithm, the minimum required time step value Δt^n_{min} should be initially compared with the initial time step value Δt^o. If Δt^n_{min} is less than Δt^o, Δt^n_{min} will be checked against the previous time step value Δt^n, and then the new time step value Δt^{n+1} will be calculated using Δt^n and Δt^n_{min} as noted in the flowchart. Otherwise, the new time step value Δt^{n+1} shall be obtained using Δt^o and Δt^n_{min}, and finally Δt^{n+1} will approach to the initial time step value Δt^o. This algorithm should be used at each time step in order to regularly update the time step value avoiding extreme changes which may lead to numerical

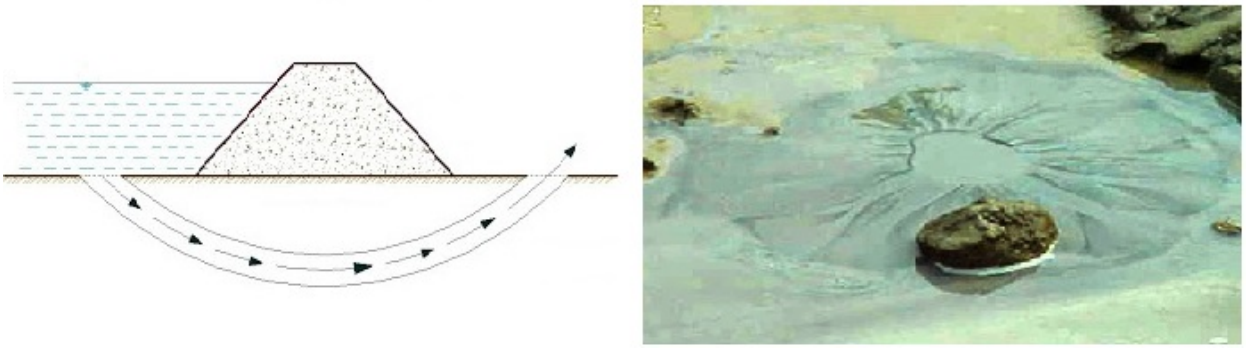

Figure 2: Schematic view of piping failure in dams

Table 1: Material properties of the fluidized bed problem

			Filter 1	Filter 2	Filter 3
Layer height	H	cm	2.5	2.5	10.5
Dry unit weight	γ	kN/m^3	15.7	15.7	14.5
Porosity (Average)	n		0.36	0.36	0.41
Friction angle	ϕ	$degree$	-	-	22
Effective diameter	D_e	mm	3	2	0.51

instabilities.

3. Modelling and simulation

An open source code, called PersianSPH[1], has been developed in C++ on Linux platform, and is used in this study. Detailed discussions to the concepts on how artificial stress and viscosity [6, 31], different types of the boundary conditions [14], soil-water interaction [14], initial in-situ stress condition [4], and the integration scheme [15] are introduced and treated in the SPH code are provided in Gholami Korzani et al. [14]. Three different geotechnical problems will be introduced and discussed in Sec. 4. As these problems are different in details, the modelling approach and initial conditions are explained individually for each problem.

4. Results and discussion

4.1. Fluidized bed problem

The processes associated with the fluidized bed problem are well-known in chemical engineering [25], where fluidized beds are beneficially used, for example, in minerals processing. However in dam engineering, the occurrence of a local fluidized bed (Fig. 2 right) at the downstream side of, for example, a levee (Fig. 2 left) is the initiation of a chain of processes leading to the so-called piping problem which can cause the failure of the complete structure. Piping is initially triggered by the fluidization of soil particles at the ground surface, which means in the condition of zero effective stress, under the influence of an upwards directed seepage flow. The existence of the fluidized bed becomes visible as a sand volcano or sand boil at the ground surface where it forms a local sink-hole. This hole then grows within the foundation in upstream direction creating finally a pipe which means a hydraulic connection with the reservoir [11, 27, 44–46].

In order to simulate the initiation of a fluidized bed and the corresponding changes in porosity, experimental investigations have been conducted with a simplified physical model (Fig. 3 left). The dimensions of

[1] http://korzani.wixsite.com/persiansph

the model and the material parameters are provided in Tab. 1. Filters 1 and 2 are used only for homogenizing the flow conditions while Filter 3 was subjected to fluidization. As an initial condition, equal hydraulic heads were applied at the top and bottom of the sample (no flow condition). Flow was applied by gradually rising the hydraulic head at the bottom of the sample (hydraulic head controlled test). The hydraulic head was increased by $1cm$ per minute until first signs of a fluidization became visible. This head was then kept constant to reach an equilibrium stage indicated by a constant thickness of the fluidized bed.

For the sake of computational efficiency, in the numerical simulation the thicknesses of the individual filter layers were reduced to 1.25, 1.25 and $2.5cm$ for Filter 1, 2 and 3, respectively (Fig. 3 right). Filter 1 and 2 were modelled with fixed in place particles. The upward flow was generated by gradually increasing flow velocity (flow rate controlled simulation) using in-flow and out-flow boundary condition as explained in [15]. Periodic boundary condition was applied to the vertical walls to eliminate the effects of the wall boundaries. This type of boundary condition was implemented by linking particles located at a boundary to particles at the opposite boundary. As a result, a particle that leaves a boundary immediately re-enters at the opposite boundary with the same velocity [13]. In total, 7500 SPH particles with a smoothing length of $0.0012m$ were deployed to simulate this problem. Darcy's law in conjunction with the Kozeny-Carman equation (Eqs. (13) and (14)) was employed to determine the changes in hydraulic conductivity with changing porosity.

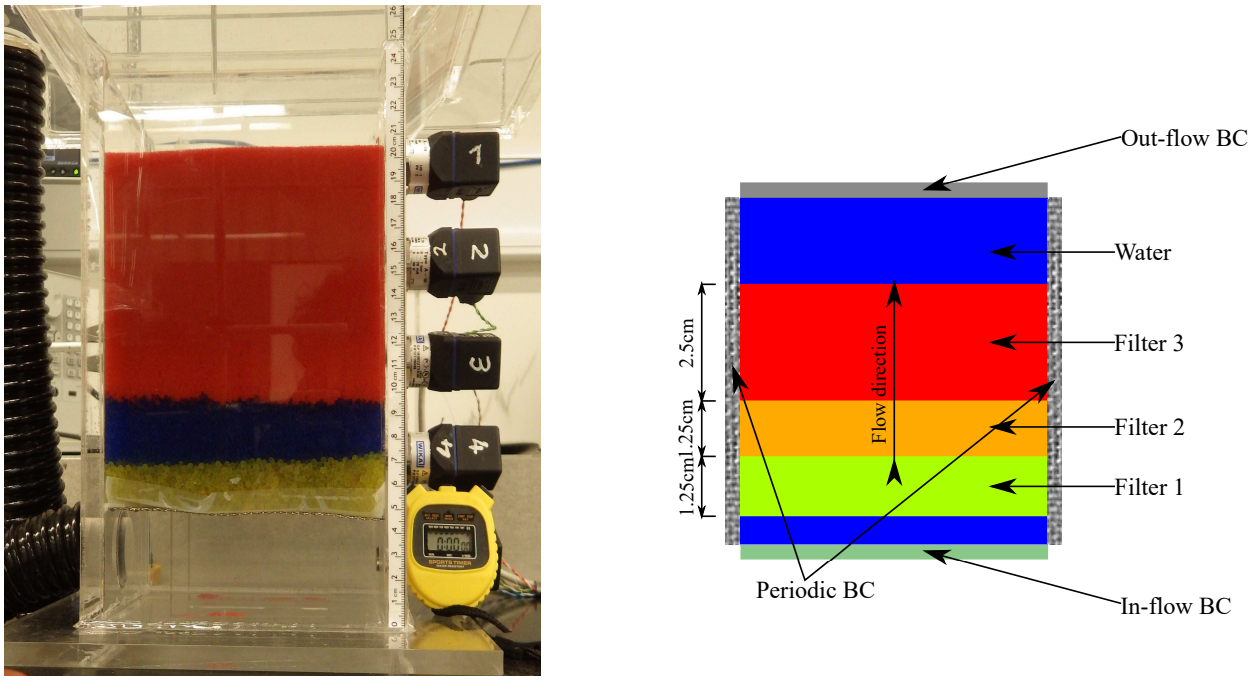

experimental setup

Schematic numerical setup

Figure 3: Experimental setup and schematic of the numerical model showing the initial condition for the fluidized bed problem

Observations during the experiment included measurements of the flow rate, changes in the height of the sample and the implementation of electromagnetic measurements [43] with the aim to derive a relationship between the dielectric permittivity and porosity. Since experiments were done in a hydraulic head controlled condition, the corresponding flow rate for the threshold of the fluidization could not be measured, and the fluidization occurred while the flow rate was rising from $0.07l/s$ to $0.12l/s$. In the experiments, the hydraulic head was kept constant until a stable height of the fluidized bed could be observed. This situation was used as the benchmark for the numerical simulation. The measured porosity in the experiment at the flow rate of $0.12l/s$ was 0.51.

In the numerical simulation, the flow rate increased linearly at in-flow boundary from 0 to $0.12l/s$ within 12 seconds. This flow rate was maintained until the end of the simulation when a steady state was achieved.

As shown in Fig. 4a, the final mean value for the porosity based on the proposed constitutive relationship is 0.508 which is in good agreement with the experimental result. Furthermore, the calculated porosity using the numerical results based on the thickness of the fluidized bed is about 0.513, which matches with the obtained porosity using the proposed constitutive relationship. The corresponding permeability for this porosity was measured in the experiments to be $9 \times 10^{-9} m^2$, while the numerically simulated value was $8 \times 10^{-10} m^2$.

Fig. 4b illustrates that the mean vertical effective stress in Filter 3 approaches values close to zero as a result of the increasing flow rate. The velocity, with which the fluidized particles move vertically upwards, reaches its maximum when the vertical effective stress is at its minimum. After this point, the velocity decreases and oscillates around zero indicating a situation of a constant thickness of the fluidized bed. It is remarkable that the vertical effective stress at this stage is not zero and oscillates around a value of approximately one-third of the initial effective stress. The flow rate at the time of the fluidization was about $0.96 l/s$ which lies between 0.07 and $0.12 l/s$.

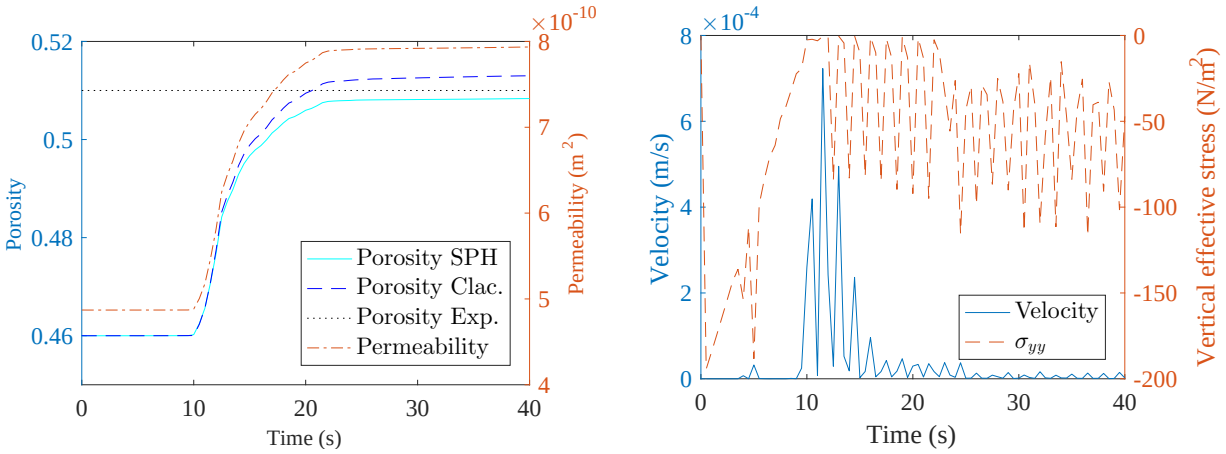

(a) Porosity and permeability

(b) Soil particles velocity and effective stress

Figure 4: Numerical results of the fluidized bed problem

The good agreement between the experimental and numerical results clearly shows that SPH is capable of reproducing the effects of flowing water on the deformation of soils and the coupling with the hydraulic conductivity. Based on the Kozeny-Carman equation, the parameter a in Eq. (13) reduced with increasing porosity. As a consequence, the seepage force using Eq. (13), which is the only force in the model moving soil particles upward, gradually decreases until equilibrium between this force and the gravity force is reached. If the permeability and porosity had been considered to be a constant in the numerical simulation, the seepage force would remain unchanged, and all soil particles would continually move upwards until they are washed out of the domain. Although the Reynolds number in this problem was around 2.7, which is within the acceptable range of Darcy's law, it should be noted that Darcy's law is commonly applied to soil with a solid skeleton. It is of course a valid question, whether the application of Darcy's law for simulating a fluidized bed problem is justified. However, already in the past Darcy's law has been applied with sedimentation tests to determine an equivalent hydraulic conductivity. Nevertheless, the presented example of a fluidized bed shows that SPH can principally be used for simulating geotechnical failures associated with the fluidized bed problem.

4.2. Overtopping of the core within rockfill dams

Failures of dams can result in catastrophic consequences especially in less developed countries as they can entail the devastation of infrastructure and agricultural land as well as the loss of precious water resources and the access to electricity. Extreme weather events leading to floods are becoming more frequent, and the increasing number of critical situations of dams and the occurrences of dam failures, such as of the

Banquiao Dam [22, 38] and the Tous Dam [1, 37], evidently demonstrate the threat emanating from these extreme situations. In the light of these failures and the prospect that climate change may further increase the number of extreme weather events, engineers need to revisit design criteria of dams and re-investigate the behaviour of existing dams for extreme hydraulic and meteorologic events. There are various breaching mechanisms involved in the failure of dams [26, 39] which can lead to the final collapse of e.g. a rockfill dam in only a few hours [50]. In order to provide the best possible preparedness against the consequences of dam failures and for maximizing protection of people and properties, the quantification of the temporal evolution of a dam failure including flooding of the affected area is of paramount importance. Accurate numerical tools capable of simulating the formation and evolution of the breach within a dam are highly beneficial for this task and can help investigating the failure and post-failure mechanisms of these water retaining structures.

A failure scenario that has been paid little attention so far is the overtopping of a core of a rockfill dam within the dam structure. In order to investigate the mechanisms associated with this failure scenario, laboratory investigations on a technical scale have been conducted in [20]. In these experiments, the core was considered to be fixed and undeformable forming the upstream boundary of the experiment. As a consequence, only the downstream slope was physically built of gravel with an inclination $1.5H : 1V$ (see Fig. 5a). Water could enter this slope only by flowing over the core (Fig. 5b) from whereon it flew vertically along the core until it reached the waterproof base. With increasing cumulative flow, a parabolic phreatic surface developed with water leaving the slope at the downstream side toe. The flow force created by the water seeping out of the slope eventually reached a critical value where particles are dislodged for the first time finally leading to a local transport of gravel particles and a subsequent failure of the downstream side slope. The result of these experiments were analyzed visually in terms of local deformation of the slope. In order to provide a more quantified value for the evolution of the deformation of the slope, a B parameter was measured throughout the test, which defines the horizontal distance between the position of last particle movements in the slope of the dam and the original position of toe of the slope (see also Fig. 6). Tests with two flow rates of $Q = 19.36l/s$ and $Q = 30.45l/s$ are considered and analyzed in this study. The properties of the used gravel are provided in Tab. 2.

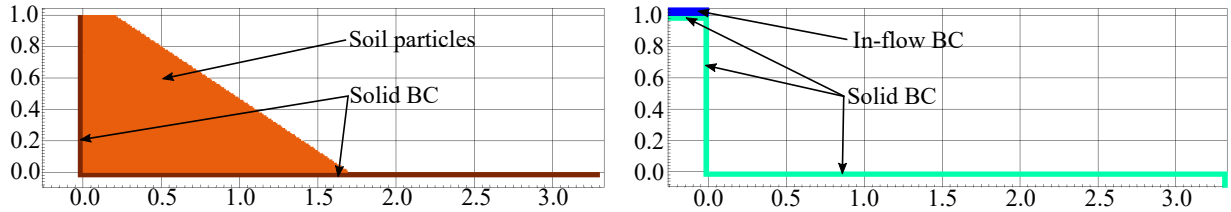

(a) Soil phase model (b) Water phase model

Figure 5: Schematic numerical model for the overtopping of the core dam (all units are in meters)

Table 2: Properties of the rockfill material

Description	Symbol	Unit	Value
Dry density	ρ_d	kg/m^3	1490
Saturated density	ρ_s	kg/m^3	1910
Porosity	n		0.41
Friction angle	ϕ	$degree$	41
Particle diameter	D_{15}	mm	25.5

The representation of the geometric condition in the numerical model is connected to problems related to the constitutive relationships used for simulating the behaviour of the gravel. The trapezoidal shape of the slope of the embankment especially under consideration of the inclination of the slope (Fig. 5a) will lead to the development of tensile stresses in the SPH soil particles in the corner of the crest of the embankment.

Table 3: Comparison of the calculated B parameter with the experimental data

$Q(l/s)$	B_{exp} (m)	Larese et al [20]		This study	
		B_{num} (m)	Error(%)	B_{num} (m)	Error(%)
19.36	0.32	0.76	137	0.317	0.9
30.45	0.68	0.90	32	0.697	2.5

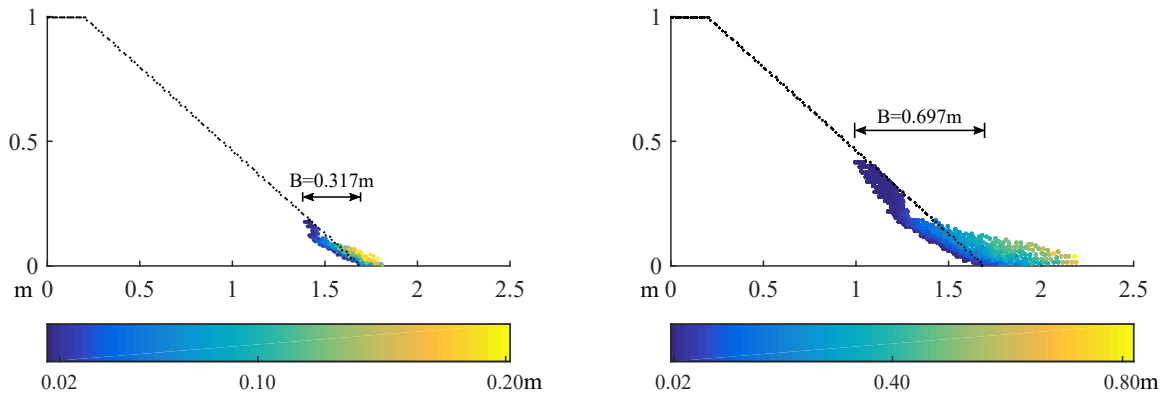

(a) $Q = 19.36l/s$ (b) $Q = 30.45l/s$

Figure 6: Result from numerical simulations using SPH: Displacement contour plot together with measured B parameter (unit is meters)

Since gravel is modelled as a non-cohesive material (Tab. 2), the embankment would have an instantaneous failure with the applied initial geometric condition even without the impact of water. In order to avoid this problem, the gravel is modelled with some minor initial cohesion which is assumed to vanish as soon as SPH soil particles get in touch with water. A parametric study showed that this initial cohesion had only a small influence on the final result of the simulation. Therefore, the minimal value of this study, $1.5kPa$, was used as initial cohesion and kept constant for the rest of the simulations. The introduction of a small cohesion to stabilize the geometry of the model as the initial condition can be justified through the fact that an effective cohesion is frequently used to mathematically describe the frictional behaviour of granular materials. No-slip solid boundary condition was applied to model solid walls, and the in-flow boundary condition was employed to generate the overtopping flow (Fig. 5b, [14]). As the gravel has a high hydraulic conductivity, the Forchheimer equation with the coefficients after Den Adel (Eqs. (13) and (15)) was used to simulate the seepage force. Approximately 12300 SPH particles with the smoothing length of $0.015m$ were initially employed.

This smoothing length representing the discretization size needs to be chosen much smaller (in this case with a factor of minimum 20) than the expected total deformation, in order to be able to accurately simulate deformation.

Fig. 6 shows the contour of the displacement and the measured B parameter at steady state for the both simulated flow rates. The finally obtained porosity and the water level within the embankment at steady state are given in Fig. 7. The numerically achieved values for the B parameter are compared in Tab. 3 with experimental results and the numerical solutions published in [20]. The results from SPH almost perfectly match with the experimental data with the largest error less than 2.5%. The fact that only particle transport at the downstream side toe takes place without causing a slope failure is connected to the shear strength parameters associated with the soil at dry and submerged condition. The dry region of the embankment is stable by assigning the small cohesion. The submerged zoned consists of interior confined section and the toe. Based on the Drucker-Prager yield criterion, the interior confined section is stable because of high

vertical stress while the toe is deforming to reach stable condition due to the loss of the cohesion and the applied seepage force. The outcome of this study shows that the presented SPH scheme is not only capable of qualitatively representing the large deformation during failure of geotechnical structures, but also can provide quantitative information on the developing shape of these structures during the failure.

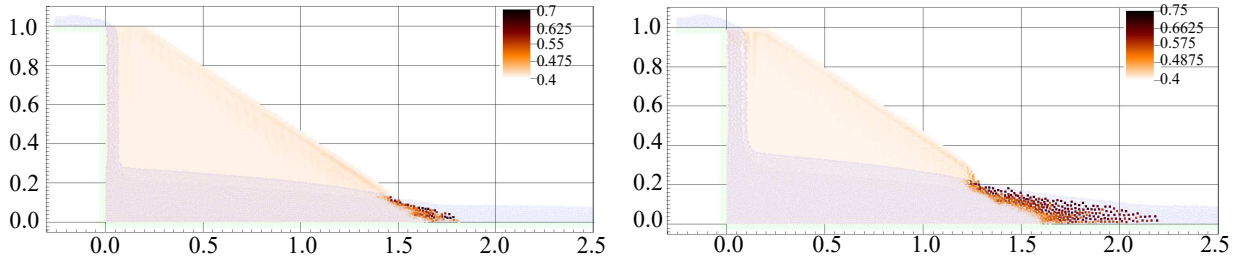

(a) $Q = 19.36l/s$ (b) $Q = 30.45l/s$

Figure 7: Porosity contour plot (light to dark brown for increasing porosity) and phreatic surface (light blue)

4.3. Hydraulic heave in excavation pits

Inner-city construction projects frequently require deep excavations into the aquifer with depths far below the ground water table. As the lowering of the water table would lead to extensive settlements around the excavation pit with consequential damages to existing structures, walls and floor of the pit must be designed in a way to withstand the water pressures and hydraulic gradients created by the head difference outside and inside the excavation pit. Frequently sheet piles are used to build the pit wall with bonding length large enough to reduce the hydraulic gradients in the floor [2] avoiding hydraulically induced failures such as hydraulic heave, uplift, and internal erosion [18]. Numerous recommendations and national guidelines are available to properly design excavation pits [2, 18, 49]. However, as the occurrence of hydraulically induced failures are strongly dependent on the geology of the surrounding ground, which in many cases is difficult to predict, and since the failures can occur instantaneous with almost no indicators, accurate numerical solutions can help to reduce uncertainty and to optimize the design [3]. Furthermore, these numerical tools can help improving our understanding of the mechanisms involved in hydraulically induced failures and the resulting consequences for the overall structure.

In order to physically visualize the hydraulic heave problem in an excavation pit, small-scaled experiments have been conducted in a tank with the dimensions 50x30x30cm for length, height and depth (Fig. 9). A model sheet pile wall with 1cm thickness was fixed in the middle of the tank forming a gap of 3cm between the end of wall and base of the tank. The tank was filled with 7cm of sand on the both sides of the wall which means that the bonding length of the wall into the sand was 4cm. An additional gravel layer with 7cm thickness was placed upstream on the sand layer (the right-hand side). The water table at upstream and downstream sides are 30 and 8cm, respectively. Initially, a weight was placed on the sand layer at the downstream side to avoid the initiation of the failure. The test started by removing the weight. Tab. 4 summarizes the material properties of the materials used in this test and used for the back analysis using SPH. Note that sand and gravel friction angles were not measured experimentally. Therefore, a sensitivity analysis was conducted to obtain appropriate friction angles and to minimize the error between experiment and numerical result.

Numerical simulations representing the situation in the tank have been carried out using the presented SPH scheme. All walls were considered to be no-slip solid BC with respect to the both phases. Darcy's law was used to model the flow within the sand layer, and Forchheimers law was applied to describe the flow in the gravel layer. In total, 27276 SPH particles with a smoothing length of 0.003m were employed. With ongoing simulation, the number of particles decreased as water particles gradually left the domain at the downstream end to imitate the hole-patterned wall at the left-hand side of the apparatus.

In the experiment, the complete failure occurred after 4.4s. A sensitivity study was carried out to find the friction angles for the sand and the gravel which best match this failure time. Fig. 8shows the result

Table 4: Properties of the materials used in the hydraulic heave problem

Description	Symbol	Unit	Sand	Gravel
Saturated density	ρ_s	kg/m^3	1975	1975
Porosity	n		0.35	0.35
Friction angle	ϕ	$degree$	29	40
Particle diameter	D_{15}	mm	-	8
Particle diameter	D_e	mm	0.8	-

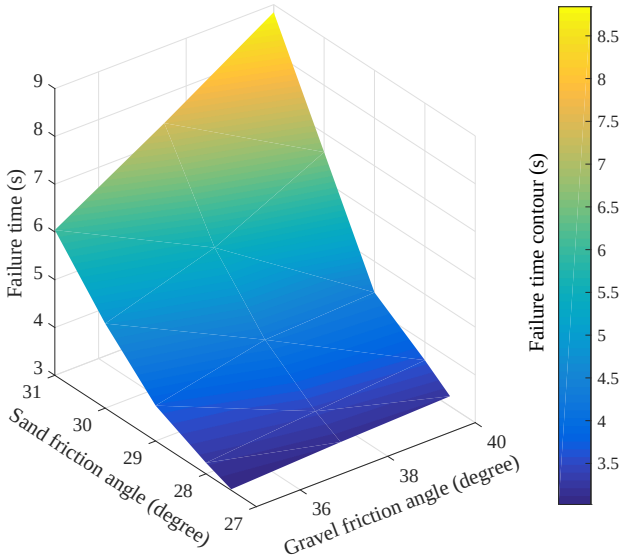

Figure 8: Numerical failure time in various friction angles for the sand and gravel

of the sensitivity analysis with the optimal friction angles for the sand and gravel of 29 and 40 degrees, respectively. Using these values, the temporal evolution of the failure was simulated. Fig. 9 shows in sequences the simulation results in comparison with the results of the experiment. As can be seen from this comparison, shape and area of the invading gravel layer into the sand layer on the upstream side of the wall are different in the numerical modelling result compared to the observations in the experiment.

For a more quantitative comparison, the temporal development of the hydraulic head and the advancement of the bottom end of the gravel layer in vicinity of the sheet wall was compared with the experimental observations. As demonstrated in Fig. 10, the falling of the hydraulic head during the test matched well with the experimental result. The simulation of the movement of the gravel layer into the sand layer, however, shows some discrepancies in comparison with the experiment, but still with an overall satisfying agreement. Nevertheless, the numerical results fairly agree with the experimental observations, which is another reference to the capabilities of the numerical scheme to adequately predict the temporal evolution of complex hydro-mechanical processes.

5. Conclusions

A numerical approach is presented for studying the hydro-mechanical behaviour of earthen structures built of moderate to high permeable soils under consideration of changes in permeability. This approach was implemented in an open-source code called PersianSPH[1], which is a numerical tool based on Smoothed

[1]http://korzani.wixsite.com/persiansph

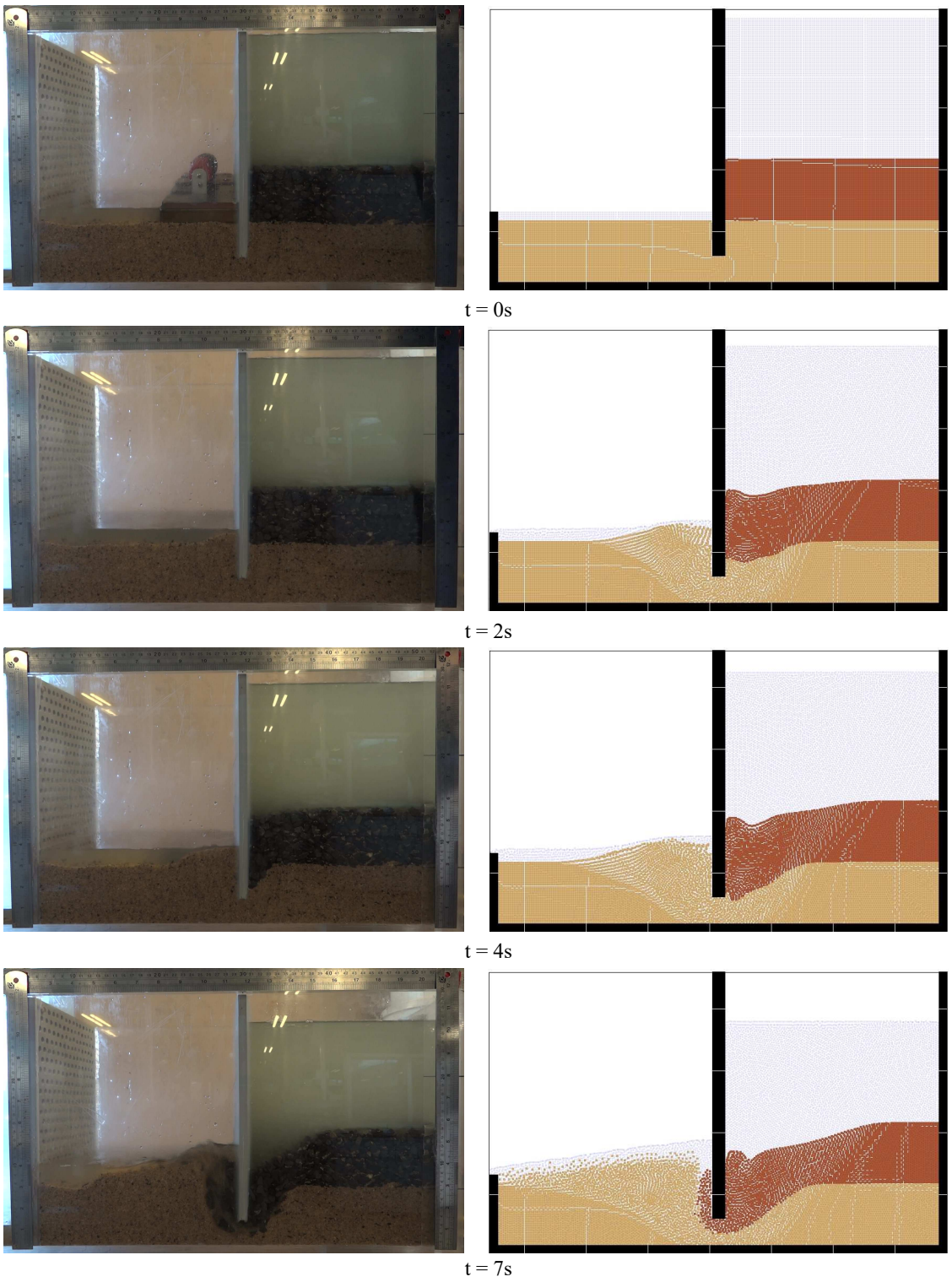

Figure 9: A comparison between the numerical simulation (right-hand side) and experimental result (left-hand side) in the different times for the hydraulic heave problem

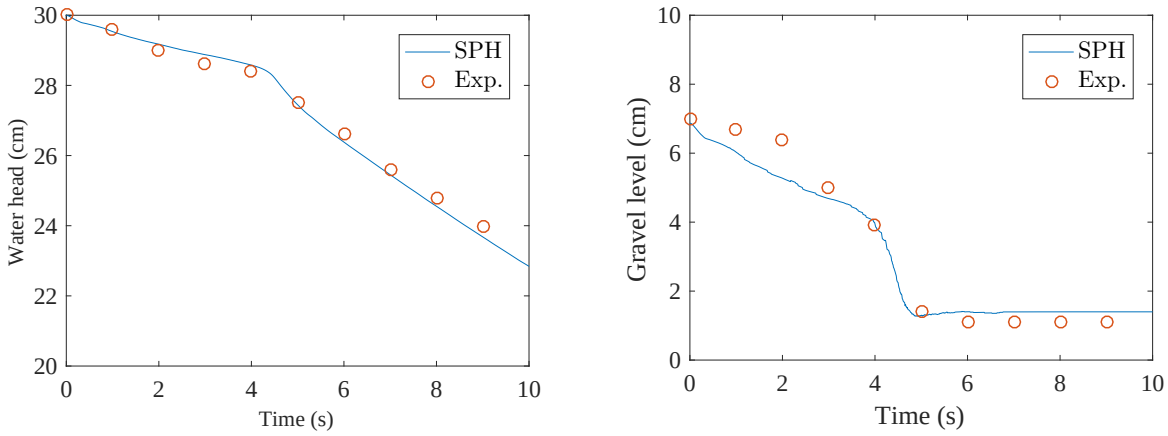

(a) The hydraulic head vs. time

(b) The bottom level of the gravel layer close to the wall vs. time

Figure 10: The overall hydraulic head and the advancement of the gravel layer in wall vicinity during the simulation

Particle Hydrodynamics (SPH) for geotechnical investigations [14, 15]. The characteristics of the presented approach can be summarized as follows:

- It employs the volumetric strain to calculate the porosity based on an initial porosity value, and accordingly update the permeability.
- In the soil-water interaction, the seepage force dynamically varies due to changes in the permeability as well as flow conditions.

The concept of a variable permeability introduced in this paper for SPH improves the modelling of the temporal evolution of a failure processes involving hydraulically induced soil deformation and to simulate the complete progress from initiation to the failure of a geotechnical structure in a more representative way. Furthermore, a correction for selecting an optimal time step value is provided since changes in the time step value during a simulation can generate numerical instabilities and errors. An algorithm is proposed to smoothly modify the time step value over the whole simulation duration.

Three distinct problems were studied in this paper to investigate the applicability, accuracy, and stability of the proposed SPH concept:

- Firstly, a fluidized bed problem was simulated and compared to experimental results. The comparison shows that the obtained porosities are in good agreement with the measured experimental results.
- The second problem concerned the overtopping of the core of a rockfill dam by water. The proposed concept in SPH was compared with experimental results published by Larese et al. [20]. A quantitative comparison was done in terms of the starting point of the slope failure. The discrepancy between experimental and numerical results was less than 2.5%.
- Finally, the development of a hydraulic heave in an excavation pit was simulated and compared with experimental results conducted in the frame of this study. The time for reaching the failure was used to back analyse the parameters of the soils. The temporal evolution of two features of the problem showed a satisfying agreement between numerical solution and the experimental result.

The presented results show that the introduced SPH framework with the proposed variable permeability concept is capable of adequately simulating the hydraulic and mechanical processes in geotechnical structures beyond the failure with satisfying accuracy.

Acknowledgements

The presented research is funded by the Australian Research Council Discovery Project, Hydraulic Erosion of Granular Structures: Experiments and Computational Simulations (DP120102188). The authors would like to thank Tilman Binttner to provide us his experimental results for the fluidized bed test. The second author would like to acknowledge the support from the Advance Queensland Fellowship program (Grant number AQ-15188).

References

[1] F. Alcrudo and J. Mulet. Description of the tous dam break case study (spain). *Journal of Hydraulic Research*, 45(sup1): 45–57, 2007.

[2] B. Aulbach, M. Ziegler, and H. Schüttrumpf. Design aid for the verification of resistance to failure by hydraulic heave. *Procedia Engineering*, 57:113–119, 2013.

[3] H. H. Bui. *Lagrangian mesh-free particle method (SPH) for large deformation and post-failure of geomaterial using elasto-plastic constitutive models*. Phd thesis, Ritsumeikan University, 2007.

[4] H. H. Bui and R. Fukagawa. An improved sph method for saturated soils and its application to investigate the mechanisms of embankment failure: Case of hydrostatic pore-water pressure. *International Journal for Numerical and Analytical Methods in Geomechanics*, 37(1):31–50, 2013.

[5] H. H. Bui, K. Sako, and R. Fukagawa. Numerical simulation of soil–water interaction using smoothed particle hydrodynamics (sph) method. *Journal of Terramechanics*, 44(5):339–346, 2007. ISSN 0022-4898.

[6] H. H. Bui, R. Fukagawa, K. Sako, and S. Ohno. Lagrangian meshfree particles method (sph) for large deformation and failure flows of geomaterial using elastic-plastic soil constitutive model. *International Journal for Numerical and Analytical Methods in Geomechanics*, 32(12):1537–1570, 2008. ISSN 03639061 10969853. doi: 10.1002/nag.688.

[7] W.-F. Chen and E. Mizuno. *Nonlinear analysis in soil mechanics*. Elsevier Amsterdam, 1990. ISBN 0444430431.

[8] W. Dehnen and H. Aly. Improving convergence in smoothed particle hydrodynamics simulations without pairing instability. *Monthly Notices of the Royal Astronomical Society*, 425(2):1068–1082, 2012. ISSN 0035-8711.

[9] H. Den Adel. Analysis of permeability measurements using forchheimers equation. Technical report, TU Delft, 1986.

[10] Y. Di and T. Sato. Liquefaction analysis of saturated soils taking into account variation in porosity and permeability with large deformation. *Computers and Geotechnics*, 30(7):623 – 635, 2003. ISSN 0266-352X. doi: http://dx.doi.org/10.1016/S0266-352X(03)00060-0.

[11] R. Fell, C. F. Wan, J. Cyganiewicz, and M. Foster. Time for development of internal erosion and piping in embankment dams. *Journal of geotechnical and geoenvironmental engineering*, 129(4):307–314, 2003.

[12] M. Gholami Korzani, S. A. Galindo-Torres, D. Williams, and A. Scheuermann. Numerical simulation of tank discharge using smoothed particle hydrodynamics. *Applied Mechanics and Materials*, 553:168–173, 2014. ISSN 3038350680. doi: 10.4028/www.scientific.net/AMM.553.168.

[13] M. Gholami Korzani, S. Galindo Torres, A. Scheuermann, and D. J. Williams. Smoothed particle hydrodynamics into the fluid dynamics of classical problems. *Applied Mechanics and Materials*, 846:73–78, 2016. ISSN 3038355283.

[14] M. Gholami Korzani, S. Galindo Torres, A. Scheuermann, and D. J. Williams. Smoothed particle hydrodynamics for investigating hydraulic and mechanical behaviour of an embankment under action of flooding and overburden loads. *Computers and Geotechnics*, 2017.

[15] M. Gholami Korzani, S. A. Galindo-Torres, A. Scheuermann, and D. J. Williams. Parametric study on smoothed particle hydrodynamics for accurate determination of drag coefficient for a circular cylinder. *Water Science and Engineering*, 10 (2):143–153, 2017. ISSN 1674-2370. doi: 10.1016/j.wse.2017.06.001.

[16] J. Grabe and B. Stefanova. Numerical modeling of saturated soils, based on smoothed particle hydrodynamics (sph). *geotechnik*, 37(3):191–197, 2014. ISSN 01726145. doi: 10.1002/gete.201300024.

[17] J. Gray, J. Monaghan, and R. Swift. Sph elastic dynamics. *Computer methods in applied mechanics and engineering*, 190 (49):6641–6662, 2001. ISSN 0045-7825.

[18] HTG. *Recommendations of the Committee for Waterfront Structures Harbours and Waterways: EAU 2012*. John Wiley & Sons, 2015.

[19] J. K. L. Lobovsky. Smoothed particle hydrodynamics modelling of fluids and solids. *Applied and Computational Mechanics*, 1:10, 2007.

[20] A. Larese, R. Rossi, E. Oñate, M. Á. Toledo, R. Morán, and H. Campos. Numerical and experimental study of overtopping and failure of rockfill dams. *International Journal of Geomechanics*, 15(4):04014060, 2013. ISSN 1532-3641.

[21] S. Li and W. K. Liu. *Meshfree particle methods*. Springer, Berlin; New York, 2004. ISBN 3540222561 (hd. bd.).

[22] D. Liu, L. Pang, and B. Xie. Typhoon disaster in china: prediction, prevention, and mitigation. *Natural Hazards*, 49(3): 421–436, 2009.

[23] G. R. Liu and M. B. Liu. *Smoothed particle hydrodynamics: a meshfree particle method*. World Scientific, New Jersey, 2005. ISBN 9812384561.

[24] L. B. Lucy. A numerical approach to the testing of the fission hypothesis. *The astronomical journal*, 82:1013–1024, 1977. ISSN 0004-6256.

[25] A. Lyngfelt, B. Leckner, and T. Mattisson. A fluidized-bed combustion process with inherent co 2 separation; application of chemical-looping combustion. *Chemical Engineering Science*, 56(10):3101–3113, 2001.

[26] T. C. MacDonald and J. Langridge-Monopolis. Breaching charateristics of dam failures. *Journal of Hydraulic Engineering*, 110(5):567–586, 1984.
[27] F. Mercier, S. Bonelli, F. Golay, F. Anselmet, P. Philippe, and R. Borghi. Numerical modelling of concentrated leak erosion during hole erosion tests. *Acta Geotechnica*, 10(3):319–332, Jun 2015. ISSN 1861-1133. doi: 10.1007/s11440-014-0349-5.
[28] J. Monaghan. Smoothed particle hydrodynamic simulations of shear flow. *Monthly Notices of the Royal Astronomical Society*, 365(1):199–213, 2006. ISSN 1365-2966.
[29] J. J. Monaghan. Smoothed particle hydrodynamics. *Annual review of astronomy and astrophysics*, 30:543–574, 1992. ISSN 0066-4146.
[30] J. J. Monaghan. Simulating free surface flows with sph. *Journal of computational physics*, 110(2):399–406, 1994. ISSN 0021-9991.
[31] J. J. Monaghan and H. Pongracic. Artificial viscosity for particle methods. *Applied Numerical Mathematics*, 1(3):187–194, 1985.
[32] J. P. Morris, P. J. Fox, and Y. Zhu. Modeling low reynolds number incompressible flows using sph. *Journal of computational physics*, 136(1):214–226, 1997. ISSN 0021-9991.
[33] M. Mukhlisin, M. R. Taha, and K. Kosugi. Numerical analysis of effective soil porosity and soil thickness effects on slope stability at a hillslope of weathered granitic soil formation. *Geosciences Journal*, 12(4):401–410, 2008. doi: 10.1007/s12303-008-0039-0.
[34] M. Nazem, D. Sheng, J. P. Carter, and S. W. Sloan. Arbitrary lagrangianeulerian method for large-strain consolidation problems. *International Journal for Numerical and Analytical Methods in Geomechanics*, 32(9):1023–1050, 2008. ISSN 1096-9853. doi: 10.1002/nag.657. URL `http://dx.doi.org/10.1002/nag.657`.
[35] C. Peng, X. Guo, W. Wu, and Y. Wang. Unified modelling of granular media with smoothed particle hydrodynamics. *Acta Geotechnica*, 11(6):1231–1247, Dec 2016. ISSN 1861-1133. doi: 10.1007/s11440-016-0496-y.
[36] H. Sabetamal, M. Nazem, J. Carter, and S. Sloan. Large deformation dynamic analysis of saturated porous media with applications to penetration problems. *Computers and Geotechnics*, 55:117 – 131, 2014. ISSN 0266-352X. doi: http://dx.doi.org/10.1016/j.compgeo.2013.08.005.
[37] A. Serra-Llobet, J. D. Tàbara, and D. Sauri. The tous dam disaster of 1982 and the origins of integrated flood risk management in spain. *Natural hazards*, 65(3):1981–1998, 2013.
[38] Y. Si. The worlds most catastrophic dam failures. *Qing (1998a)*, pages 25–38, 1998.
[39] M. Toledo. Safety of rockfill dams subject to overtopping. In *International Symposium on New Trends and Guidelines on Dam Safety, L. Berga, ed., Taylor & Francis, London*, 1998.
[40] T.-L. Tsai and W.-S. Jang. Deformation effects of porosity variation on soil consolidation caused by groundwater table decline. *Environmental Earth Sciences*, 72(3):829–838, 2014. ISSN 1866-6299. doi: 10.1007/s12665-013-3006-7.
[41] M. R. A. Van Gent. Stationary and oscillatory flow through coarse porous media. Technical report, TU Delft, 1993.
[42] D. Violeau and A. Leroy. On the maximum time step in weakly compressible sph. *Journal of Computational Physics*, 256:388–415, 2014. ISSN 0021-9991. doi: 10.1016/j.jcp.2013.09.001.
[43] N. Wagner, M. Schwing, and A. Scheuermann. Numerical 3-d fem and experimental analysis of the open-ended coaxial line technique for microwave dielectric spectroscopy on soil. *IEEE Transactions on Geoscience and Remote Sensing*, 52 (2):880–893, 2014. ISSN 0196-2892. doi: 10.1109/TGRS.2013.2245138.
[44] C. F. Wan and R. Fell. Investigation of rate of erosion of soils in embankment dams. *Journal of geotechnical and geoenvironmental engineering*, 130(4):373–380, 2004.
[45] C. F. Wan and R. Fell. Laboratory tests on the rate of piping erosion of soils in embankment dams. *Geotechnical Testing Journal*, 27(3):1–9, 2004.
[46] C. F. Wan and R. Fell. *Experimental investigation of internal instability of soils in embankment dams and their foundations*. University of New South Wales, School of Civil and Environmental Engineering, 2004.
[47] H. Wang. *Theory of linear poroelasticity with applications to geomechanics and hydrogeology*. Princeton University Press, 2000.
[48] H. Wang and W. Xu. Relationship between permeability and strain of sandstone during the process of deformation and failure. *Geotechnical and Geological Engineering*, 31(1):347–353, 2013. ISSN 1573-1529. doi: 10.1007/s10706-012-9588-0.
[49] R.-B. Wudtke. Failure mechanisms of hydraulic heave at excavations. In *19th European young geotechnical engineers conference, Gyor, Hungary*, 2008.
[50] Y. Xu and L. Zhang. Breaching parameters for earth and rockfill dams. *Journal of Geotechnical and Geoenvironmental Engineering*, 135(12):1957–1970, 2009.
[51] X. Yang, M. Liu, and S. Peng. Smoothed particle hydrodynamics modeling of viscous liquid drop without tensile instability. *Computers & Fluids*, 92(0):199–208, 2014. ISSN 0045-7930. doi: 10.1016/j.compfluid.2014.01.002.
[52] W. Zhang, K. Maeda, H. Saito, Z. Li, and Y. Huang. Numerical analysis on seepage failures of dike due to water level-up and rainfall using a water–soil-coupled smoothed particle hydrodynamics model. *Acta Geotechnica*, 11(6):1401–1418, Dec 2016. ISSN 1861-1133. doi: 10.1007/s11440-016-0488-y.